Fast Time-Resolved Magnetic Optical Rotatory Dispersion Measurements. 1. Mueller Analysis of Optical and Photoselection-Induced Artifacts

Raymond M. Esquerra, Robert A. Goldbeck,* Daniel B. Kim-Shapiro,† and David. S. Kliger

Department of Chemistry and Biochemistry, University of California at Santa Cruz, Santa Cruz, California 95064

Received: March 31, 1998; In Final Form: August 28, 1998

A simple and sensitive near-null technique for multichannel nanosecond time-resolved magnetic optical rotatory dispersion measurements is introduced with a theoretical analysis describing the basis of the technique and the effects of optical imperfections, photoselection-induced linear dichroism and birefringence, and the Faraday rotation of the solvent and cell windows. This treatment identifies a potential artifact in photolyzed samples that is associated with the coupling of photoselection-induced linear dichroism with the solvent−cell Faraday rotation. Excitation geometries that minimize this problem are described. Experimental applications of the technique to the ligand rebinding reaction of myoglobin−CO after ligand photolysis are presented in the following article.

Introduction

The simple and sensitive technique for multichannel, nanosecond time-resolved magnetic optical rotary dispersion (TRMORD) measurements presented here is similar to a technique developed previously in this laboratory to measure nanosecond natural time-resolved optical rotatory dispersion (TRORD),[1] except that the TRMORD technique incorporates a magnetic field at the sample and a Faraday compensator to distinguish the Faraday rotation of the solvent from that of the sample. The basic optical principle of the TRORD/TRMORD technique is a near-null polarimetric method, first described by Keston and Lospalluto,[2] that has been used previously for single-wavelength, microsecond TRORD measurements.[3,4] The nanosecond TRMORD technique is also closely related to a near-null ellipsometric technique developed in this laboratory to measure nanosecond time-resolved magnetic circular dichroism (TRMCD).[5,6] Although MCD is studied more often than MORD, MCD being more easily interpreted than MORD, TRMORD may, nevertheless, be preferred over the ellipsometric MCD technique as a time-resolved measure of magnetic optical activity because it requires fewer optical components and presents potential signal-to-noise advantages.[1] We present a derivation of the optical principle of the technique and investigate possible artifacts and their amelioration, particularly those associated with photoselection-induced ordering of the sample. An application of the technique to the study of the microsecond to millisecond kinetics of ligand rebinding after ligand photolysis of the carbonyl adduct of horse skeletal myoglobin is discussed in the following article.

Magnetic optical rotation (Faraday effect) and magnetic circular birefringence (MCB) are closely related (circular birefringence, the phase difference between circular polarization components, is equal to twice the observed optical rotation), and both terms may be used to describe the dispersive part of magnetic optical activity. We shall generally use MCB in this paper when describing magnetic optical activity as an extensive quantity and MORD when referring to an intensive quantity. Thus, MORD is used in this work when the rotation is expressed as the specific magnetic rotation or as the specific molar magnetic rotation, and MCB is used for the phase difference in radians or degrees per unit field. With MCB expressed in degrees, MORD is defined as

$$[\mathrm{MORD}]_{\mathrm{sp}} = \frac{\mathrm{MCB}}{2cd} \tag{1}$$

$$[\mathrm{MORD}]_{\mathrm{mol}} = \frac{\mathrm{MCB}}{cd}\frac{M}{200} \tag{2}$$

where c is the concentration in grams per milliliter, d is the path length in decimeters, M is the solute molecular weight, and the subscripts sp and mol denote the specific magnetic rotation and the specific molar magnetic rotation, respectively.[7] The corresponding natural ORD terms have analogous definitions.

Signal Analysis

As in the near-null measurement of natural ORD,[1,2] an MORD measurement is made by placing a sample between two crossed polarizers and then rotating one polarizer, first clockwise (facing the probe source) and then counterclockwise, by a small angle β from the crossed position. The signal is defined as the difference of the detected intensities for the clockwise and counterclockwise positions, normalized to their sum,

$$s_{\mathrm{D}}(t) = \frac{I_{+\beta}(t) - I_{-\beta}(t)}{I_{+\beta}(t) + I_{-\beta}(t)} \tag{3}$$

* Corresponding author. E-mail: goldbeck@chemistry.ucsc.edu. Fax: (831) 459-2935.

† Present address: Department of Physics, Wake Forest University, Winston-Salem, NC 27109-7507.

10.1021/jp981693x CCC: $15.00
Published on Web 10/14/1998

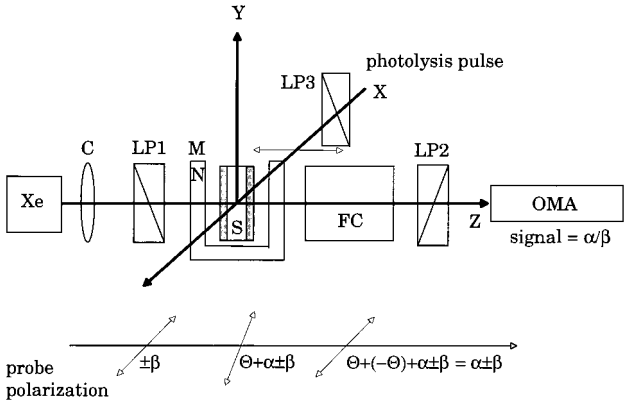

Figure 1. Schematic diagram of the optical layout of a near-null instrument for TRMORD measurements using a crossed pump−probe geometry: Xe, xenon flashlamp; CL, collimating lens; LP1, LP2, LP3, linear polarizers; M, magnet with field collinear with the probe propagation direction; S, sample; FC, Faraday compensator; OMA, optical multichannel analyzer; Θ, magnetic optical rotation of solvent and windows (an optical rotation of Θ is applied in the opposite direction by the Faraday compensator); $\pm\beta$, small rotation angle of polarizer; α, natural and magnetic optical activity of the sample; signal, ratio of difference to the sum of intensities for $\pm\beta$ polarizer rotations; *X*, *Y*, *Z*, laboratory coordinates. The open-headed arrows indicate the polarization direction of the probe light. LP1 transmits probe light polarized along the *X* axis, LP2 is polarized along the *Y* axis, and LP3 polarizes the excitation beam in the Z direction.

where the subscript D denotes the direction of the magnetic field, parallel (P) or antiparallel (A) with respect to the probe propagation direction. It is simple to show that this signal is proportional to the MCB of the sample, for small MCB. Using the small-angle approximation, the intensity transmitted through crossed polarizers is proportional to the square of the total rotation $(H(\mathrm{MCB})/2 \pm \beta)^2$ for a parallel field of strength *H*. Thus

$$s_{\mathrm{p}}(t) = \frac{-\beta H(\mathrm{MCB})}{\beta^2 + {}^1/_4 H^2(\mathrm{MCB})^2} \cong \frac{-H(\mathrm{MCB})}{\beta} \tag{4}$$

for $H(\mathrm{MCB}) \ll \beta$, where we assume that the Faraday rotation contribution of the solvent and cell windows is canceled by an additional optical device, a Faraday compensator, placed between the polarizers. (For single-wavelength measurements, an appropriate rotation of one of the polarizers suffices to cancel the solvent−cell Faraday rotation. Faraday compensators for multichannel measurements are described in the following article.) A schematic description of the changes in the plane of polarization of the probe light during a near-null MORD measurement is shown in Figure 1. Below, we present a full Mueller calculus analysis of the technique incorporating the Faraday effect of the solvent and its cancellation with a Faraday compensator.

This technique measures the total optical rotation regardless of its source. Thus, both natural and magnetic CB are measured in chiral samples. However, because the MCB changes sign upon reversal of the magnetic field direction, CB and MCB can be separated by performing a measurement at opposite field directions. That is,

$$s_{\mathrm{p}} = -(\mathrm{CB} + H(\mathrm{MCB}))/\beta$$
$$s_{\mathrm{A}} = -(\mathrm{CB} - H(\mathrm{MCB}))/\beta \tag{5}$$

where *H* is the magnetic field intensity in Teslas. CB and MCB are isolated as

$$\mathrm{CB}(t) = -\beta(s_{\mathrm{p}}(t) + s_{\mathrm{A}}(t))/2$$
$$\mathrm{MCB}(t) = -\beta(s_{\mathrm{p}}(t) - s_{\mathrm{A}}(t))/(2H) \tag{6}$$

with circular birefringence expressed in radians.

Mueller Calculus. The notation used here is similar to that in optical analyses presented previously for near-null measurements of time-resolved linear dichroism[8] and TRMCD.[9] The intensity and polarization state of light is represented as a Stokes vector

$$\mathbf{S} = \begin{pmatrix} S_1 \\ S_2 \\ S_3 \\ S_4 \end{pmatrix} \tag{7}$$

where S_1, S_2, S_3, and S_4 are the total intensity, difference in intensities polarized along the vertical and horizontal directions, the difference in intensities polarized at ±45° with respect to the vertical direction, and the difference in intensities between left and right circularly polarized light, respectively. The normalized Stokes vector for unpolarized light is $S_1 = 1$ and $S_2 = S_3 = S_4 = 0$.

A 4 × 4 Mueller matrix

$$\mathbf{M} = \begin{pmatrix} \mathrm{M}_{11} & \mathrm{M}_{12} & \mathrm{M}_{13} & \mathrm{M}_{14} \\ \mathrm{M}_{21} & \mathrm{M}_{22} & \mathrm{M}_{23} & \mathrm{M}_{24} \\ \mathrm{M}_{31} & \mathrm{M}_{32} & \mathrm{M}_{33} & \mathrm{M}_{34} \\ \mathrm{M}_{41} & \mathrm{M}_{42} & \mathrm{M}_{43} & \mathrm{M}_{44} \end{pmatrix} \tag{8}$$

describes the effect of an optical element on the polarization state of incident light as

$$\mathbf{S}^{\mathrm{f}} = \mathbf{M}\mathbf{S}^{\mathrm{i}} \tag{9}$$

and for *N* optical elements as

$$\mathbf{S}^{\mathrm{f}} = \mathbf{M}^N\mathbf{M}^{N-1} \ldots \mathbf{M}^1\mathbf{S}^{\mathrm{i}} = \mathbf{M}^{\mathrm{total}}\mathbf{S}^{\mathrm{i}} \tag{10}$$

The final state of light is given by $\mathbf{S}^{\mathrm{f}}$. (Only the first element, the total intensity, is typically measured directly by detectors, e.g., photomultipliers.)

Linear Polarizers. The Mueller matrix for a linear polarizer is shown in Chart 1, where $t_{\max}$ is the maximum transmission and *r* is the extinction ratio ($r \equiv t_{\min}/t_{\max}$).[10] The angle θ is the azimuthal angle defined by the angle between the transmission axis and the laboratory *X* axis (horizontal).

Stray Linear Birefringence. The general Mueller matrix for a uniaxial linear birefringent element is shown in Chart 2, where φ and δ are the azimuthal angle and the retardance, respectively.[10]

CHART 1

$$\mathbf{M}^{\mathrm{LP}} = \frac{f_{\max}}{2}\begin{pmatrix} 1+r & (1-r)\cos 2\theta & (1-r)\sin 2\theta & 0 \\ (1-r)\cos 2\theta & (1-r^{1/2})^2\cos^2 2\theta + 2r^{1/2} & (1-r^{1/2})^2\sin 2\theta \cos 2\theta & 0 \\ (1-r)\sin 2\theta & (1-r^{1/2})^2\sin 2\theta \cos 2\theta & (1-r^{1/2})^2\sin^2 2\theta + 2r^{1/2} & 0 \\ 0 & 0 & 0 & 2r^{1/2} \end{pmatrix} \tag{11}$$

CHART 2

$$\mathbf{M}^{\mathrm{LB}} = \begin{pmatrix} 1 & 0 & 0 & 0 \\ 0 & \cos^2 2\phi + \sin^2 2\phi \cos\delta & \sin 2\phi \cos 2\phi(1-\cos\delta) & -\sin 2\phi \sin\delta \\ 0 & \sin 2\phi \cos 2\phi(1-\cos\delta) & \sin^2 2\phi + \cos^2 2\phi \cos\delta & \cos 2\phi \sin\delta \\ 0 & \sin 2\phi \sin\delta & -\cos 2\phi \sin\delta & \cos\delta \end{pmatrix} \tag{12}$$

Sample. In the most general case, a sample can exhibit linear dichroism, linear birefringence, circular dichroism, and circular birefringence. The general Mueller matrix for a sample can be written as

$$\mathbf{M}^{\mathrm{s}} = \mathrm{e}^{-A}(\mathbf{I} - \mathbf{F} + {}^1/_2\mathbf{F}^2 - ...) \tag{13}$$

where **I** is the unit matrix and

$$\mathbf{F} = \begin{pmatrix} 0 & \mathrm{LD} & \mathrm{LD}' & -\mathrm{CD} \\ \mathrm{LD} & 0 & -\mathrm{CB} & -\mathrm{LB}' \\ \mathrm{LD}' & \mathrm{CB} & 0 & \mathrm{LB} \\ -\mathrm{CD} & \mathrm{LB}' & -\mathrm{LB} & 0 \end{pmatrix} \tag{14}$$

with

$$A = 1.151(A_x + A_y)$$
$$\mathrm{LD} = 1.151(A_x - A_y)$$
$$\mathrm{LD}' = 1.151(A_{45^\circ} - A_{135^\circ})$$
$$\mathrm{LB} = 2\pi(n_x - n_y)d/\lambda$$
$$\mathrm{LB}' = 2\pi(n_{45^\circ} - n_{135^\circ})d/\lambda$$
$$\mathrm{CD} = 1.151(A_{\mathrm{l}} - A_{\mathrm{r}})$$
$$\mathrm{CB} = 2\pi(n_{\mathrm{l}} - n_{\mathrm{r}})d/\lambda \tag{15}$$

expressed in radians. A, λ, n, and d are the absorbance, wavelength, refractive index, and path length, respectively.[11−13] The subscripts denote the polarization direction of the incident light, with the subscripts l and r specifying left and right circular polarization. Each of the 16 elements of $\mathbf{M}^{\mathrm{s}}$ is given by an infinite series containing products of linear and circular effects. If LD, LD′, LB, and LB′ are small (optically thin sample), then it is useful to consider only the first three terms of eq 13

$$\mathbf{M}_{11}{}^{\mathrm{s}} = \frac{\mathrm{e}^{-A}}{2}(2 + \mathrm{CD}^2 + \mathrm{LD}^2 + \mathrm{LD}'^2)$$
$$\mathbf{M}_{12}{}^{\mathrm{s}} = \frac{\mathrm{e}^{-A}}{2}(-2\mathrm{LD} + \mathrm{CB}\cdot\mathrm{LD}' - \mathrm{CD}\cdot\mathrm{LB}')$$
$$\mathbf{M}_{13}{}^{\mathrm{s}} = \frac{\mathrm{e}^{-A}}{2}(-2\mathrm{LD}' + \mathrm{CD}\cdot\mathrm{LB} - \mathrm{CB}\cdot\mathrm{LD})$$
$$\mathbf{M}_{14}{}^{\mathrm{s}} = \frac{\mathrm{e}^{-A}}{2}(2\mathrm{CD} + \mathrm{LD}'\cdot\mathrm{LB} - \mathrm{LD}\cdot\mathrm{LB}')$$
$$\mathbf{M}_{21}{}^{\mathrm{s}} = \frac{\mathrm{e}^{-A}}{2}(-2\mathrm{LD} + \mathrm{CD}\cdot\mathrm{LB}' - \mathrm{CB}\cdot\mathrm{LD}')$$
$$\mathbf{M}_{22}{}^{\mathrm{s}} = \frac{\mathrm{e}^{-A}}{2}(2 - \mathrm{CB}^2 + \mathrm{LD}^2 - \mathrm{LB}'^2)$$
$$\mathbf{M}_{23}{}^{\mathrm{s}} = \frac{\mathrm{e}^{-A}}{2}(2\mathrm{CB} + \mathrm{LD}'\cdot\mathrm{LD} + \mathrm{LB}\cdot\mathrm{LB}')$$
$$\mathbf{M}_{24}{}^{\mathrm{s}} = \frac{\mathrm{e}^{-A}}{2}(2\mathrm{LB}' - \mathrm{CB}\cdot\mathrm{LB} - \mathrm{CD}\cdot\mathrm{LD})$$
$$\mathbf{M}_{31}{}^{\mathrm{s}} = \frac{\mathrm{e}^{-A}}{2}(-2\mathrm{LD}' + \mathrm{CB}\cdot\mathrm{LD} - \mathrm{CD}\cdot\mathrm{LB})$$
$$\mathbf{M}_{32}{}^{\mathrm{s}} = \frac{\mathrm{e}^{-A}}{2}(-2\mathrm{CB} + \mathrm{LD}'\cdot\mathrm{LD} + \mathrm{LB}\cdot\mathrm{LB}')$$
$$\mathbf{M}_{33}{}^{\mathrm{s}} = \frac{\mathrm{e}^{-A}}{2}(2 - \mathrm{CB}^2 + \mathrm{LD}'^2 - \mathrm{LB}^2)$$
$$\mathbf{M}_{34}{}^{\mathrm{s}} = \frac{-\mathrm{e}^{-A}}{2}(2\mathrm{LB} + \mathrm{CB}\cdot\mathrm{LB}' + \mathrm{CD}\cdot\mathrm{LD}')$$
$$\mathbf{M}_{41}{}^{\mathrm{s}} = \frac{\mathrm{e}^{-A}}{2}(2\mathrm{CD} - \mathrm{LD}'\cdot\mathrm{LB} + \mathrm{LD}\cdot\mathrm{LB}')$$
$$\mathbf{M}_{42}{}^{\mathrm{s}} = \frac{-\mathrm{e}^{-A}}{2}(2\mathrm{LB}' + \mathrm{CB}\cdot\mathrm{LB} + \mathrm{CD}\cdot\mathrm{LD})$$
$$\mathbf{M}_{43}{}^{\mathrm{s}} = \frac{\mathrm{e}^{-A}}{2}(2\mathrm{LB} - \mathrm{CB}\cdot\mathrm{LB}' - \mathrm{CD}\cdot\mathrm{LD}')$$
$$\mathbf{M}_{44}{}^{\mathrm{s}} = \frac{\mathrm{e}^{-A}}{2}(2 + \mathrm{CD}^2 - \mathrm{LB}^2 - \mathrm{LB}'^2) \tag{16}$$

as presented previously by others.[13] In many cases, only the first term in the series expansion for each component of **M** needs to be considered in an optical analysis. Note that for samples that possess only one optical property, the infinite series in eq 13 can be summed to give an exact trigonometric expression, such as that in eq 12 for a linearly birefringent sample.

A magnetic field induces field-dependent terms into the linear and circular dichroisms and birefringences of the sample. Only the induced circular terms are of appreciable size,[14] and these can be incorporated into the circular dichroism and birefringence as[15]

$$\begin{aligned} \mathrm{CD} &\rightarrow \mathrm{CD} + H_{\mathrm{D}}\mathrm{MCD} \\ \mathrm{CB} &\rightarrow \mathrm{CB} + H_{\mathrm{D}}\mathrm{MCB}_{\mathrm{T}} \end{aligned} \tag{17}$$

where CD and CB now refer to the natural circular effects and

$$H_{\mathrm{D}} = H\cos\psi \tag{18}$$

ψ being the angle between the magnetic field direction and the propagation direction of the probe light. MCD and MCB are defined analogously to natural CD and CB (eq 15)

$$\begin{aligned} \mathrm{MCD} &= 1.151(A_{\mathrm{L}} - A_{\mathrm{R}})_{\mathrm{H}} \\ \mathrm{MCB} &= 2\pi d(n_{\mathrm{L}} - n_{\mathrm{R}})_{\mathrm{H}}/\lambda \end{aligned} \tag{19}$$

where the subscript H indicates the absorption or refractive difference induced by the application of a magnetic field of unit intensity. The sample solvent and cell windows, although transparent and achiral, will have a substantial MCB or Faraday effect, and consequently, the total magnetic optical rotation ($\mathrm{MCB_T}$) is

$$\mathrm{MCB_T} = \mathrm{MCB_{sample}} + \mathrm{MCB_{SW}} \tag{20}$$

where the subscript SW denotes the contribution from the solvent and cell windows.

To reduce the number of terms in the expansion, the total circular dichroism and circular birefringence for the sample will be defined as the field-dependent sum of the natural and magnetic components of the optical activity

$$\begin{aligned} \mathrm{CD_D{}^T} &= \mathrm{CD} + H_{\mathrm{D}}\mathrm{MCD_{sample}} \\ \mathrm{CB_D{}^T} &= \mathrm{CB} + H_{\mathrm{D}}\mathrm{MCB_{sample}} \end{aligned} \tag{21}$$

Henceforth, the subscript sample will be dropped and MCD and MCB will refer solely to sample properties while $\mathrm{MCB_{SW}}$ will refer to the independent contribution to the optical rotation from the windows and solvent as given in eq 20.

Due to the large disparity in concentrations, the $\mathrm{MCB_{SW}}$ term is usually much larger than MCB. However, the MCB of the sample is the desired quantity, so the MCB of the solvent and cell windows must be experimentally distinguished from that of the sample. Because of the wavelength dispersion of the solvent−cell rotation, accurate measurement of the sample MCB requires that the polarization plane of the probe light be rotated in an opposite direction by an angle equal in magnitude to the solvent−cell rotation at each measurement wavelength. This counterrotation is accomplished by a Faraday compensator.

Faraday Compensator. The Mueller matrix for an ideal Faraday compensator is

$$\mathbf{M}^{\mathrm{FC}} = \begin{pmatrix} 1 & 0 & 0 & 0 \\ 0 & \cos \mathrm{FC} & -\sin \mathrm{FC} & 0 \\ 0 & \sin \mathrm{FC} & \cos \mathrm{FC} & 0 \\ 0 & 0 & 0 & 1 \end{pmatrix} \tag{22}$$

where FC is the total wavelength-dependent optical rotation of the Faraday compensator from any combination of natural CB or MCB.[9] (Note that the optical rotation of the Faraday compensator, FC, is defined in eq 22 with a sense of rotation opposite to that for the natural CB or MCB of the sample.)

MORD Measurements. The experimentally detected signal in a near-null MORD measurement is the ratio of the difference to the sum of intensities corresponding to small rotations, $\pm\beta$, of the first (horizontal) polarizer from its crossed position relative to a second (vertical) polarizer. Thus, the signal at a given magnetic field orientation, *D*, from eqs 3 and 7 is

$$s_{\mathrm{D}} = \frac{S_1(+\beta) - S_1(-\beta)}{S_1(+\beta) + S_1(-\beta)} \tag{23}$$

The measured signal calculated from eq 10 becomes

$$s_{\mathrm{D}} = \frac{\mathbf{M}^{\mathrm{LP_2}}\mathbf{M}^{\mathrm{LB_4}}\mathbf{M}_{\mathrm{D}}{}^{\mathrm{FC}}\mathbf{M}^{\mathrm{LB_3}}\mathbf{M}^{\mathrm{LB_2}}\mathbf{M}_{\mathrm{D}}{}^{\mathrm{S}}\mathbf{M}^{\mathrm{LB_1}}\Delta\mathbf{M}^{\mathrm{LP_1}}\mathrm{S}}{\mathbf{M}^{\mathrm{LP_2}}\mathbf{M}^{\mathrm{LB_4}}\mathbf{M}_{\mathrm{D}}{}^{\mathrm{FC}}\mathbf{M}^{\mathrm{LB_3}}\mathbf{M}^{\mathrm{LB_2}}\mathbf{M}_{\mathrm{D}}{}^{\mathrm{S}}\mathbf{M}^{\mathrm{LB_1}}\Sigma\mathbf{M}^{\mathrm{LP_1}}\mathrm{S}} \tag{24}$$

where Σ and Δ are the matrix sum and the matrix difference for the two polarizer orientations $\pm\beta$ and $\mathrm{LB_1}$, $\mathrm{LB_2}$, $\mathrm{LB_3}$, and $\mathrm{LB_4}$ are the linear birefringences from the front and back of the sample and compensator cells, respectively. As explained above, the measurement is performed at two magnetic field directions, P and A, to distinguish natural from magnetic rotation in chiral samples.

Ideal Case. In the ideal case, all optical elements are perfect, linear birefringence is negligible, the Faraday compensator exactly cancels the Faraday effect of the solvent and cell, and β is large compared to the optical properties of the sample. The measured signal is then

$$s_{\mathrm{D}} = \frac{-(\mathrm{LD}' + \mathrm{CB_D{}^T})}{\beta} \tag{25}$$

As β is typically much less than 1 rad, this results in a significant magnification of the optical rotation signal. In oriented samples, however, this method detects not only the optical rotation but also the diagonal component of linear dichroism, as shown in eq 25. In isotropic samples, which do not exhibit linear dichroism, the measured signal reduces to

$$s_{\mathrm{D}} = \frac{-\mathrm{CB_D{}^T}}{\beta} \tag{26}$$

in agreement with the heuristic derivation presented in eq 4. The induced linear dichroism of photoselected samples does not generally pose a problem for optical rotation measurements because LD′ may be made negligible with proper selection of the excitation geometry (see discussion below).

Nonideal Cases. Expanding eq 24 in terms of all the optical effects present gives a complete description of the measured signal. However, the complete expression is cumbersome and difficult to interpret, so each effect is first considered separately and then the most significant interactions between effects are

considered. We present these nonideal cases in order to examine the conditions required for an accurate measurement of the signal as given by eq 26.

Effect of Imperfect Polarizer Extinction. Neglecting other imperfections, eq 24 with finite polarizer extinction, r, becomes

$$s_D \approx \frac{-(CB_D^T)(1-r)^2\beta}{(1-r)^2\beta^2 + 2r} \approx \frac{-(CB_D^T)}{\beta + (2r/\beta)} \tag{27}$$

Equation 27 shows that finite polarizer extinction attenuates the signal and sets a limit on the minimum selection of β. Useful polarizer extinctions range from 10^{-6} to 10^{-4}, giving a minimum β range of $1-10°$ in order to obtain at least 1% accuracy in eq 27.

Signal Saturation. A Faraday compensator cancels the large Faraday effect of the solvent and cell windows. However, magnetic optical rotation from the sample itself may also be substantial in magnitude at very high fields. In this case, the measured signal becomes

$$s_D \approx \frac{-(H_D(MCB))}{\beta + (4\beta)^{-1}H_D{}^2((MCB)^2 + (MCD)^2)} \tag{28}$$

where the Faraday rotation from the sample is considered to be comparable to or larger than β. Thus, the effect of a large sample optical rotation is to attenuate the signal magnification, i.e., signal saturation. As there is a large difference in the wavelength dependence of β, MCB, and MCD, this saturation can have a wavelength dependence that distorts measured band shapes. Along with eq 27, avoidance of the signal saturation in eq 28 may also set a limit on the minimum selection of β. As an example, for a sample rotation of 100 mdeg, a β value of at least 1° is required to keep attenuation below 1%.

Effects of Imperfect Faraday Compensation, Polarizer Misalignment, and Imperfect Polarizer Rotations. Three cases are presented in this section: (1) rotations to plus and minus angles not exactly equal in magnitude to β, (2) polarizers not perfectly crossed, and (3) Faraday effect of the solvent and cell not exactly canceled. Cases 1 and 2 are combined in eq 29 (the second-order circular terms in the denominator of eq 28 are neglected for clarity)

$$s_D \approx \frac{-(CB_D^T - 2\phi - \delta)}{\beta + \delta + (2\beta)^{-1}[\phi^2 + (\phi+\delta)^2 - (2\phi+\delta)(CB_D^T)]} \tag{29}$$

where the first polarizer is oriented at ϕ from horizontal, the second is at 90°, and the measurement rotations are done at $\beta + \delta$ and $-\beta$. That is, the polarizers are ϕ degrees from crossed and the measurement rotations are unsymmetrical by δ. By setting either δ or ϕ equal to zero, the effects of each separate misalignment can be determined. These imperfections shift the baseline and lead to an attenuation of the signal. Because both result from a misaligned polarizer, they have identical, usually constant, wavelength dependences.

For case 3, the measured signal becomes

$$s_D \approx \frac{-(CB_D^T) + \Delta}{\beta + (4\beta)^{-1}[(CB_D^T + \Delta)^2 + (CD_D^T)^2]} \tag{30}$$

with

$$\Delta = H_D(MCB_{SW}) - FC \tag{31}$$

Equation 30 shows that imperfect cancellation causes a baseline shift and an attenuation of the signal. The magnitude of the shift is proportional to the difference between the rotations associated with MCB_{SW} and the Faraday compensator. In the case of a Faraday compensator comprising a solvent blank in an identically homogeneous field, this difference is proportional to any difference in field strength and has a wavelength variation that is given approximately by the Drude equation.[16] However, if there are differences in composition of the solvent and cell in the sample and compensator or if the natural ORD of a chiral solution is used as the Faraday compensator, then there will be a more complicated wavelength dependence to the shift in eq 31. As one approaches an absorption band, this effect becomes more pronounced and can be approximated by using separate Drude equations for the solvent−cell and the FC. Assuming a single transition dominates the Drude equation for each, we get

$$\Delta \propto \frac{(\lambda_{SW}{}^2 - \lambda_{FC}{}^2)}{(\lambda^2 - \lambda_{SW}{}^2)(\lambda^2 - \lambda_{FC}{}^2)} \tag{32}$$

where the subscripted λ's denote absorption wavelengths for the solvent and cell windows (SW) or the Faraday compensator material (FC) and the magnitudes of the rotations for SW and FC are equal by construction at wavelengths far from the absorption wavelengths.

Field Inhomogeneity. This section describes the effect of field inhomogeneity on near-null MORD measurements. Field inhomogeneity can affect such MORD measurements when the Faraday rotation of the solvent−cell and the optical rotation of the Faraday compensator vary differently over the cross section of the probe beam, as when magnets for the sample and Faraday compensator have different field homogeneities or when a chiral sample is used to compensate a nonuniform sample field. Although the Faraday rotation may cancel on average over the cross section of the beam, the quadratic term in Δ in eq 30 will not generally average to zero in the presence of field inhomogeneities, as shown below.

The paths of the probe light through the sample and the FC are described as cylinders with lengths equal to the path lengths of the sample cell and FC and diameters equal to that of the probe beam. The signal (for a homogeneous sample), averaged over the cross section and path length of a uniform and collimated probe beam, is

$$s_D \approx \frac{-\left(CB + \left\langle \frac{MCB}{a}\int_0^a H_D(r,\theta,z)\,dz \right\rangle + \langle\Delta\rangle\right)}{\beta + (4\beta)^{-1}[\langle B\rangle + \langle G\rangle]} \tag{33}$$

where

$$\langle\Delta\rangle = \left\langle \frac{MCB_{SW}}{a}\int_0^a H_D(r,\theta,z)\,dz - \frac{1}{b}\int_0^b FC(r,\theta,z)\,dz \right\rangle \tag{34a}$$

$$B = \left\langle \left(CB + \frac{MCB + MCB_{SW}}{a}\int_0^a H_D(r,\theta,z)\,dz - \frac{1}{b}\int_0^b FC(r,\theta,z)\,dz \right)^2 \right\rangle \tag{34b}$$

and

$$G = \left\langle \left(\mathrm{CD} + \frac{\mathrm{MCD}}{a} \int_0^a H_\mathrm{D}(r,\theta,z)\, \mathrm{d}z \right)^2 \right\rangle \tag{34c}$$

$H_\mathrm{D}(r,\theta,z)$ and $\mathrm{FC}(r,\theta,z)$ are the distributions in cylindrical coordinates, centered on the light beam, of the magnetic field and Faraday compensator, respectively. The averaging, indicated by brackets, is defined by

$$\langle f(r,\theta.z) \rangle \equiv \frac{1}{\pi R^2} \int_0^{2\pi} \mathrm{d}\theta \int_0^R [f(r,\theta,z)] r\, \mathrm{d}r \tag{34d}$$

The path lengths of the sample and Faraday compensator are a and b, respectively, and the radius of the probe beam is R. (Differences in the contributions of cell materials and solvent to $\mathrm{MCB_{SW}}$ and FC are neglected for simplicity).

Consider an example in which the magnetic field of the sample and the Faraday compensator have small radially symmetric inhomogeneities. That is,

$$H_\mathrm{D}(r,\theta,z) = H_0(1 - hr^2)\cos\psi \tag{35}$$

$$\mathrm{FC}(r,\theta,z) = \mathrm{FC}_0(1 - fr^2) \tag{36}$$

where H_0 and FC_0 are the respective field magnitudes at the center of the probe beam. The value of FC_0 giving average cancellation of Δ (for a parallel longitudinal field, $\psi = 0$) is found by solving

$$\langle \Delta \rangle = \left\langle \frac{\mathrm{MCB_{SW}}}{a} \int_0^a H_\mathrm{D}(r,\theta,z)\, \mathrm{d}z - \frac{1}{b} \int_0^b \mathrm{FC}(r,\theta,z)\, \mathrm{d}z \right\rangle = 0 \tag{37}$$

which yields

$$\mathrm{FC}_0 = \frac{\mathrm{MCB_{SW}} H_0 (2 - hR^2)}{(2 - fR^2)} \tag{38}$$

or

$$\mathrm{FC}_0 = \mathrm{MCB_{SW}} H_0 [1 + (f - h)R^2/2 + f(f - h)R^4/4 + ...] \tag{39}$$

Using the inhomogeneities described by eqs 35 and 36, at the value of FC_0 given by eq 38, the measured signal can be derived from eqs 33 and 34 as

$$s_\mathrm{D} \approx \frac{-(\mathrm{CB} + H_0(1 - hR^2/2)\mathrm{MCB})}{\beta \left[1 + \left(\frac{H_0 \mathrm{MCB_{SW}} (f - h) R^2}{4\sqrt{3}\beta} \right)^2 \right]} \tag{40}$$

to second order in f and h. Note that from eq 35, $H_0(1 + hR^2/2)$ is the average sample field value. Equation 40 shows that although the Faraday effect from the solvent and cell windows can be canceled in the numerator, mismatched radial inhomogeneity, $h \neq f$, attenuates the signal via the second-order term in the denominator. Equation 40 establishes the maximum relative field inhomogeneity, $(f - h)R^2$, that can be tolerated for a particular experiment: if p is the minimum detectable percent signal attenuation, then we have

$$(f - h)R^2 \lesssim (0.5\, p)^{1/2} \beta (H_0(\mathrm{MCB}_{SW}))^{-1} \tag{41}$$

As an example, for a ratio of Faraday birefringence to β of unity (a magnitude typical for a 0.5 cm path length cell in the visible spectral region, at 1 T field strength and $\beta = 1°$), a maximum inhomogeneity mismatch corresponding to 70% of H_0 could be tolerated at $p = 1\%$. Mismatch tolerances at $p = 1\%$ are plotted in Figure 2 for birefringence:β ratios up to 10.

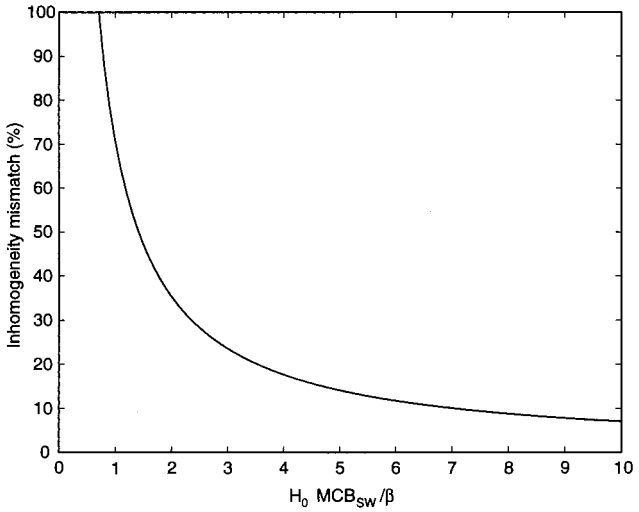

Figure 2. Percent difference in sample and compensator radial field inhomogeneities, $100(f - h)R^2$, giving a 1% signal attenuation as a function of solvent-window Faraday birefringence (in units of β).

Stray Linear Birefringence. Linear birefringence both rotates the plane of linearly polarized light and adds ellipticity to the polarization. When the linear birefringence from the optical cell windows is included in eq 24, the signal in the absence of sample orientation becomes the equation shown in Chart 3, where the ϕ's denote the orientation of the fast axis and the δ's give the retardance for each birefringent window, indicated by the numbered subscripts. Perhaps the most important feature of eq 42 is the absence of any first-order linear birefringence terms (in the sense that terms with factors that involve two small optical effects, such as CD·δ, are second order). Such first-order LB terms do appear in the ellipsometric MCD method and give it a greater sensitivity to LB artifacts than that predicted here for the MORD technique. This can result in an experimental advantage for MORD over MCD measurements in the presence of stray birefringences, whether induced by inadvertent strain, flow of anisotropic solutes, or photoselection (see below).

Equation 42 shows that stray linear birefringences cause a baseline offset and attenuate the signal (summation terms in the numerator and denominator, respectively) and that the magnitudes of these effects are proportional to the products of the retardances of the windows and their orientations. (Note that if the dispersions of the window retardances are different than that of β, the attenuation and offset of the signal will depend on the wavelength.) Hence, there is a set of orientations for uniaxially strained windows that eliminates the offset and attenuation. More significantly, the stray birefringence introduces a second-order MCD (CD) coupling term into the numerator and denominator. The MCD (CD) term in the numerator is scaled by the retardance of the first window (reflecting the fact that MCD (CD) can be measured using elliptically polarized light,[17] as window birefringence introduces ellipticity into the probe beam). The birefringence terms in the denominator are made negligible by selecting an appropriately large value of β. Similarly, the use of low-strain optics (retardance small compared to β) also reduces the effect of terms introduced by stray birefringence. Generally, high- quality optics, selection of β, and proper orientation of birefringent axes

CHART 3

$$s_D \approx \frac{-\left[CB_D{}^T + CD_D{}^T\delta_1 \cos(2\phi_1) + \frac{1}{2}\sum_{i=1}^{4}\delta_i{}^2 \cos(2\phi_i)\sin(2\phi_i) + \sum_{i=1}^{3}\sum_{j=i+1}^{4}\delta_i\delta_j \cos(2\phi_i)\sin(2\phi_j)\right]}{\beta + \frac{CD_D{}^T}{2\beta}\sum_{i=1}^{4}\delta_i \sin(2\phi_i) + (4\beta)^{-1}[(\sum_{i=1}^{4}\delta_i \sin(2\phi_i))^2 + (CB_D{}^T)^2 + (CD_D{}^T)^2]} \quad (42)$$

may all be used to reduce the influence of stray linear birefringence.

Sample Orientation and Photoselection. In many time-resolved applications, such as the one presented in the following article, the sample is photolyzed with a linearly polarized laser pulse and spectral measurements are made at various delay times after photolysis. At times that are short compared to the rotational diffusion time, incomplete photolysis produces a distribution of phototransformed molecules having a preferred orientation with respect to the polarization axis of the excitation pulse. This photoselection process results in the partial alignment of an initially isotropic sample, an alignment that eventually decays exponentially with a time constant determined by the rotational diffusion constant.[10] Thus, the possibility of photoselection effects needs to be considered in time-resolved spectroscopic measurements when the delay time is shorter than about 3 rotational diffusion lifetimes of the sample under investigation. For biological samples, this lifetime ranges from about 20 ns for myoglobin[18] to about 20 ms for the purple membrane patches of bacteriorhodopsin (bR).[19]

Faraday rotation of the pump beam will generally affect the photoselection of samples in a magnetic field, except when the beam propagation is transverse to the field. Two limiting excitation geometries are discussed here, the collinear and transverse, or crossed, geometries. We assume that the probe beam is always collinear with the applied field, so that in the crossed geometry, the excitation beam propagation axis is perpendicular to both the probe propagation axis and the field lines, whereas in the collinear geometry, all three are aligned. The polarization vector of a crossed excitation pulse can have both parallel and perpendicular components relative to the probe propagation axis, with directions and magnitudes that remain constant as the beam propagates through the field. The polarization vector of a collinear excitation pulse, being transverse to the probe-field axis, is typically determined initially by the orientation of the first polarizer in the MORD apparatus before undergoing Faraday rotation in the magnetized sample.

The signal, second order in sample optical properties (now neglecting stray window birefringence), is

$$s_D \approx -2\beta\{2(CB_D{}^T + LD') - LB(CD_D{}^T) + LD'LD + LB'LB + LD(CB_D{}^T + MCB_{SW})\}\{4\beta^2(1 + LD) + LD'^2 + LB'^2 - 2LB'(CD_D{}^T) + 2LD'(CB_D{}^T) + (CB_D{}^T)^2 + (CD_D{}^T)^2 + 2LD'(MCB_{SW})\}^{-1} \quad (43)$$

a result that can be simplified in reference to the crossed and collinear geometries described above. In the crossed geometry, if the pump beam is linearly polarized perpendicular to the probe propagation direction and forms an angle χ with the transmission axis of the first polarizer (X axis in Figure 1), then

$$LD = LD_0 \cos(2\chi) \qquad LD' = LD_0 \sin(2\chi)$$
$$LB = LB_0 \cos(2\chi) \qquad LB' = LB_0 \sin(2\chi) \quad (44)$$

where LD_0 and LB_0 are the linear dichroism and birefringence, respectively, along the laser polarization axis. The signs of LD_0 and LB_0 are determined in photolyzed samples by the relative absorptive and refractive differences between initial and excited molecules.

If χ is considered to be nearly a multiple of $\pi/2$, eq 43 becomes eq 45 shown in Chart 4, where the subscripts on LD_0 and LB_0 have been dropped. If circular effects are considered to be small relative to other optical properties, this reduces to eq 46 shown in Chart 5.

The first linear dichroism term in the numerator is the same as that in eq 25. This term is zero when the pump polarization is either perfectly parallel or perpendicular to the transmission axis of the first polarizer ($\chi = 0°$ or 90°, respectively) but can distort the shape of optical rotation spectra (and the apparent kinetics of photolyzed samples) if χ is misaligned by even a fraction of a degree, because of the large relative size of photoselection-induced LD. In any event, this term, being field independent, cancels when MCB is determined from the difference of opposed-field measurements. The third term in the numerator of eq 46 represents a coupling between the photoselection-induced linear dichroism of the sample (the component parallel to the pump polarization) and the Faraday rotation of the sample solvent and cell. This term is analogous to the coupling between MCB_{SW} and LB that appears in near-null ellipsometric measurements of MCD.[9] It arises in the same physical manner as the first-order linear dichroism term, except that rather than being caused by skewed alignment of the polarizer transmission axes and the pump polarization, it is the Faraday effect of the solvent and cell that rotates the probe polarization out of alignment with the polarizer transmission axis. Because the optical rotation of the solvent and cell can be quite large, this coupling can distort time-resolved spectral band shapes. Moreover, this term is field dependent and does not subtract from opposite-field determinations of MCB. It, thus, may complicate time-resolved MCB measurements using the crossed geometry when the pump polarization vector has components transverse to the probe propagation.

The squared terms involving LD and LB in the denominator of eq 46 can result in an attenuation of the measured signal. Thus, photoselection-induced LD and LB can cause a wavelength- and time-dependent attenuation of the signal at times before rotational diffusion is complete. Although these terms have a $\sin^2(2\chi)$ dependence and vanish when $\chi = 0°$ or 90°, these values of χ are also the orientations that maximize the contribution of the third term in the numerator of eq 46. In general, however, attenuation by the latter term can be minimized by an appropriately large selection of β. The third term in the denominator arises from coupling between the Faraday effect of the solvent−cell and the component of photoselection-induced linear dichroism that is diagonal to the pump polarization. As both factors can be large, their product can lead to distortion of the measured signal, a potential problem that can be minimized both by appropriate selection of β and by using the excitation geometry described below.

CHART 4

$$s_D \approx \frac{-\left[CB_D{}^T + \sin(2\chi)\,LD + \frac{1}{2}\cos(2\chi)(LD(CB_D{}^T + MCB_{SW}) - LB(CD_D{}^T))\right]}{\left[\beta + \frac{1}{4\beta}((CB_D{}^T)^2 + (CD_D{}^T)^2 + \sin^2(2\chi)(LD^2 + LB^2)) + \frac{1}{2\beta}\sin(2\chi)(LD(CB_D{}^T) - LB(CD_D{}^T) + MCB_{SW}(LD))\right]} \quad (45)$$

CHART 5

$$s_D \approx \frac{-\left[CB_D{}^T + \sin(2\chi)\,LD + \frac{1}{2}\cos(2\chi)\,(MCB_{SW}LD)\right]}{\beta\left[1 + \frac{1}{4\beta^2}\sin^2(2\chi)(LD^2 + LB^2) + \frac{1}{2\beta^2}\sin(2\chi)\,(MCB_{SW}(LD))\right]} \quad (46)$$

It is well-known that birefringence effects are avoided in uniaxial samples by probing along the optic axis. This uniaxial probe geometry is realized in the crossed excitation geometry by orienting the polarization of the pump beam along the probe propagation direction. In this case, the sample appears isotropic to the probe beam and the measurement is free by symmetry from the orientation effects described above.[20] (The following article demonstrates measurements using isotropic excitation as well as the effects of anisotropic excitation described by eq 46.) This uniaxial probe geometry is also achieved (on average over the path length) when a circularly or randomly polarized collinear excitation beam is used. However, the presence of linear polarizers in the probe-beam path makes such collinear polarization geometries difficult to implement, because optics to circularly polarize or depolarize laser light typically have stray linear birefringence and cannot be placed between crossed polarizers without interfering with a near-null measurement.

We briefly consider collinear excitation with a linearly polarized beam for which the polarization direction is determined by the first (probe beam) polarizer. Faraday rotation of the probe and excitation beams generally complicates the signal description in this case because the beam polarizations are functions of path length and wavelength. Probe and pump polarizations will diverge as the beams travel through the magnetized sample and the Faraday compensator unless their wavelengths are identical, in which case the beams are rotated identically at a given path length.

Finally, we consider the combined effects of stray linear birefringences and oriented sample birefringence and dichroism. With the same restrictions as those used in the derivation of eqs 42 and 46, the signal is given by

$$s_D \approx -\Bigg\{CB_D{}^T + \sin(2\chi)\,LD + (CD_D{}^T - LB\cos(2\chi))\delta_1 \times \cos(2\phi_1) - \sum_{i=2}^{4} LB\sin(2\chi)\delta_i\sin(2\phi_i) - \frac{1}{2}\cos(2\chi)\,(LB(CD_D{}^T) - LD(CB_D{}^T + MCB_{SW})) + \frac{1}{2}\sum_{i=1}^{4}\delta_i{}^2\cos(2\phi_i)\sin(2\phi_i) + \sum_{i=1}^{3}\sum_{j=i+1}^{4}\delta_i\delta_j\cos(2\phi_i)\sin(2\phi_i)\Bigg\}\Bigg\{\beta + \frac{1}{4\beta}((CD_D{}^T)^2 + (CB_D{}^T)^2 + \sin^2(2\chi)(LD^2 + LB^2)) + \frac{(CD_D{}^T - LB\cos(2\chi))}{2\beta}\sum_{i=1}^{4}\delta_i \times \sin(2\phi_i) + \frac{1}{2\beta}\sin(2\chi)(LD(CB_D{}^T) - LB(CD_D{}^T)) + \frac{1}{4\beta}\Big(\sum_{i=1}^{4}\delta_i\sin(2\phi_i)\Big)^2\Bigg\}^{-1} \quad (47)$$

where the lowest order couplings between LB and LD, the birefringence and dichroism of oriented samples, and the window birefringences, δ_i, now appear as the third and fourth terms in the numerator and as a similar term in the denominator. (An additional term that is second order in the δ_i's is also retained in the denominator for completeness.)

Summary

We have presented a detailed theoretical analysis of a near-null polarimetric technique for MORD measurements, addressing, in particular, photoselection-induced artifacts that may affect nanosecond and faster time-scale measurements on photolyzed samples. This analysis shows that the MORD signal is effectively amplified by the use of a small β value (cf. eq 4), which provides the signal to instrumental noise ratio needed for nanosecond time scale measurements with bright but relatively unstable light sources such as flashlamps. The price paid for this amplification is a greater sensitivity to linear dichroism in ordered samples. (Although this situation is an improvement over that for the near-null ellipsometric MCD method. The latter method has a greater sensitivity to linear birefringence, which being more spectrally dispersed than linear dichroism is more likely to interfere with measurements within absorption bands than is a dichroism artifact likely to interfere with measurements of circular birefringence in the MORD method.) In particular, it may be necessary to consider the effects of photoselection-induced orientation after photoexcitation, even for initially isotropic samples, if such measurements are made at times before rotational diffusion of the sample is complete. The (photoselection-induced) linear dichroism term that then appears to first order in near-null natural ORD measurements can be canceled in MORD by subtracting opposing-field measurements, but the second-order term coupling solvent−cell Faraday rotation with the sample's linear dichroism does not cancel in MORD. However, this artifact is found to be minimized by a uniaxial pump−probe geometry, i.e., by aligning the photoselection-induced optical axis with the probe propagation axis, an arrangement that is also stable to first order with respect to angular misalignments.[21] Finally, we also find that a minimum level of field homogeneity is required for accurate near-null MORD measurements (a condition that does not appear in conventional polarimetric MORD methods), although this requirement is not found to be very severe at typical field strengths. In the following article, we present experimental demonstrations of these results and an application to the kinetics of ligand rebinding and protein relaxation after myoglobin−CO photolysis.

Acknowledgment. We thank Drs. Jim Lewis and Diping Che for stimulating discussions on polarization spectroscopy. This work was supported by the National Institute of General

Medical Sciences, Grant No. GM38549 (D.S.K.). D.B.K.-S. also acknowledges the support of an NIH postdoctoral fellowship, HL08969.

References and Notes

(1) Shapiro, D. B.; Goldbeck, R. A.; Che, D.; Esquerra, R. M.; Paquette, S. J.; Kliger, D. S. *Biophys. J.* **1995**, *68*, 326−334.

(2) Keston, A.; Lospalluto, J. *Fed. Proc.* **1953**, *12*, 229.

(3) Carapellucci, P. A.; Richtol, H. H.; Strong, R. L. *J. Am. Chem. Soc.* **1967,** *89*, 1742−1743.

(4) Tsuda, M. *Photochem. Photobiol.* **1979**, *29*, 175−177.

(5) Goldbeck, R. A.; Dawes, T. D.; Milder, S. J.; Lewis, J. W.; Kliger, D. S. *Chem. Phys. Lett.* **1989**, *156*, 545−549.

(6) Goldbeck, R. A.; Dawes, T. D.; Einarsdóttir, Ó.; Woodruff, W. H.; Kliger, D. S. *Biophys. J.* **1991**, *66*, 125−134.

(7) Shashoua, V. E. *Methods Enzymol.* **1973**, *27*, 796−810.

(8) Che, D.; Shapiro, D. B.; Esquerra, R. M.; Kliger, D. S. *Chem. Phys. Lett.* **1994**, *224*, 145−154.

(9) Che, D.; Goldbeck, R. A.; McCauley, S. W.; Kliger, D. S. *J. Phys. Chem.* **1994**, *98*, 3601−3611.

(10) Kliger, D. S.; Lewis, J. W.; Randall, C. E. *Polarized Light in Optics and Spectroscopy*; Academic: San Diego, CA, 1990.

(11) Jensen, H. P.; Schellman, J. A.; Troxell, T. *Appl. Spectrosc.* **1978**, *32*, 192−200.

(12) Schellman, J. A. In *Polarized Spectroscopy of Ordered Systems*; Saori, B., Thulstrup, E. W., Eds.; Kluwer Academic: Dordrecht, 1988; p 231.

(13) Schellman, J. A.; Jensen, H. P. *Chem. Rev.* **1987**, *87*, 1359−1399.

(14) Michl, J.; Thulstrup, E. W. *Spectroscopy with Polarized Light*; VCH: New York, 1986; Chapter 1.

(15) Landau, L. D.; Lifshitz, E. M. *Electrodynamics of Continuous Media*, 2nd ed.; Pergamon: New York, 1984; Chapter 101.

(16) Barron, L. D. *Molecular Light Scattering and Optical Activity*; Cambridge University: Cambridge, 1982; Chapters 1, 6−7.

(17) Lewis, J. W.; Tilton, R. F.; Einterz, C. M.; Milder, S. J.; Kuntz, I. D.; Kliger, D. S. *J. Phys. Chem.* **1985**, *89*, 289−294.

(18) Jones, C. M.; Ansari, A.; Henry, E. R.; Christoph, G. W.; Hofrichter, J.; Eaton, W. A. *Biochemistry* **1992**, *31*, 6692−6702.

(19) Esquerra, R. M.; Che, D.; Shapiro, D. B.; Lewis, J. W.; Bogomolni, R. A.; Fukushima, J.; Kliger, D. S. *Biophys. J.* **1996**, *70*, 962−970.

(20) We neglect the possible direct effect of photoselection-induced orientation on the magnitude of the measured MOA. The dependence on the excitation-probe geometry of such orientation effects is predicted to be generally different than that of the photoselection-induced LB and LD artifacts considered here, see: Goldbeck, R. A.; Che, D.; Kliger, D. S. *J. Chem. Phys.* **1996**, *104*, 6930−6937.

(21) Björling, S. C.; Goldbeck, R. A.; Milder, S. J.; Randall, C. E.; Lewis, J. W.; Kliger, D. S. *J. Phys. Chem.* **1991**, *95*, 4685−4694.